CrossMark

REGULAR ARTICLE

Structural and electronic properties of lead sulfide quantum dots from screened hybrid density functional calculations including spin–orbit coupling effects

Antonio M. Márquez[1] · Laura C. Pacheco[1] · Javier Fdez. Sanz[1]

Abstract We present in this work density functional theory calculations of the structural and electronic properties of $(PbS)_n$ nanoparticles with $n = 4$–32. Particular care has been taken on the correct description of their electronic structure by using a hybrid functional including the spin–orbit coupling effects. We demonstrate that the bonding in PbS nanoparticles is quite different from bulk PbS as the six Pb–S bonds around a single Pb atom are found to have a different character while in bulk PbS all Pb–S distances are equivalent. We also relate the geometric structure to the evolution of the HOMO–LUMO gaps and show how the computed electronic properties strongly depend on the functional used. Finally, based on an extrapolation of our results, we predict that to obtain the onset of absorption in the infrared region of the spectrum a cubic nanoparticle of ~1.96 nm side length is needed, a result that is in agreement with existing experimental information.

Keywords Lead sulfide · PbS nanoparticles · DFT · Spin–orbit · Structure · Absorption spectrum

1 Introduction

Lead chalcogenides quantum dots (QDs) have been extensively studied over the years in relation to their unique chemical, structural, and electronic properties compared to their bulk counterparts. The tunability of their electronic properties, related to strong quantum confinement effects arising from the restriction of the electronic wave function to limited regions of space, results in size-dependent electronic properties (see [1] and references therein). The possibility of controlling these properties makes lead chalcogenides interesting candidates for many applications, including energy storage and conversion [2, 3], optoelectronics [4], sensing [5, 6], and photocatalysis [7].

In particular, lead sulfide (PbS) quantum dots have attracted much attention in recent years in relation both to the favorable properties of bulk PbS (large Bohr radius of 18 nm, narrow band gap of 0.14 eV and high carrier mobility), the availability of synthetic routes for creating size tuned PbS QDs [8], and to their higher stability in comparison with PbSe QDs [9–11]. Notably, the thermal stability of colloidal PbS nanoparticles has been recently studied by Keitel et al. [11]. These authors have shown that, despite an increase in crystalline domain size at temperatures above 200 °C, no discernible structural changes are observed below 150 °C in PbS QDs. These data support the existence of a quite broad temperature range of PbS QDs structural stability. For these reasons, the structures and electronic properties of PbS nanoparticles have been examined, both theoretically and experimentally. However, even the most recent density functional theory calculations have been limited by using either generalized gradient approximation (GGA)-based functionals [12], which are known to underestimate the band gaps due to the self-interaction error, or by using the hybrid B3LYP exchange–correlation functional [13, 14], known to largely overestimate the band gaps and to fail in the description of metallic systems [15, 16]. Moreover, the accurate description of the electronic structure

✉ Antonio M. Márquez
marquez@us.es

[1] Departamento de Química Física, Facultad de Química, Universidad de Sevilla, 41012 Seville, Spain

of these systems requires considering the semicore Pb d states and the incorporation of the relativistic effects (spin–orbit coupling, SOC) for the valence Pb electrons [17]. Finally, these studies have been limited to compute the HOMO–LUMO gaps, and to the best of our knowledge, only one work has examined, through ab initio CID calculations, the electronic excitation spectrum of some $(PbS)_n$ nanoparticles [13]. In this regard, it is important to notice that both LDA (local density approximation) and GGA-based versions of DFT are well known for their underestimation of the HOMO–LUMO gap (the band gap in extended systems). This is related to the lack of an attractive electron–hole term in these approximations. However, the screened hybrid Heyd–Scuseria–Ernzerhof (HSE) functional has been recently shown to produce remarkably good band gaps for semiconductors and small gap insulators [16]. In particular, both LDA and GGA functionals when applied to lead chalcogenides fail to describe most of their electronic properties. However, a significant improvement is found for methods that go beyond the semilocal approximation [17]. Notably, the HSE functional produces band gaps that are in good agreement with experimental data. This has been related to the separation of the exchange energy in this functional into a short-range non-local and orbital-dependent term and the remainder, treated by a semilocal approximation [18].

Here we present, for the first time, accurate DFT calculations based on the screened hybrid Heyd–Scuseria–Ernzerhof functional including the spin–orbit coupling effects, known to significantly improve the description of bulk Pb chalcogenides with respect to standard DFT–GGA functionals, particularly electronic properties like the order of band gaps and effective carrier masses. We explore geometric parameters, bonding energies and electronic structures (HOMO–LUMO gaps and electronic absorption spectra) of $(PbS)_n$ QDs with n ranging from $n = 4$ to $n = 32$. Our results allow us to demonstrate that the bonding in $(PbS)_n$ QDs is quite different from bulk PbS as the six Pb–S distances around a single Pb atom are found to have different character while in bulk PbS all distances are equivalent. We also show how the description of the electronic properties on these systems (HOMO–LUMO gaps and electronic absorption spectra) strongly depends on the functional used. Based on an extrapolation of our hybrid density functional calculations with SOC effects, we predict that to have a HOMO–LUMO gap in the IR region of the spectrum (1.65 eV) a cubic NP of at least 1.96 nm side length will be required, a result which agrees with the experimental observation of band gap of 1.5 eV for PbS QDs of 2.6 nm diameter.

2 Computational details

The initial geometries of $(PbS)_n$ clusters ($n = 4$–32) were constructed taking as starting point the cubic arrangement of $(PbS)_4$. Larger clusters were built by adding PbS units to the lower sized clusters and, generally, maintaining the orthorhombic structure except in $(PbS)_5$ where a lower symmetry structure was found and in $(PbS)_6$ where an isomer with a C_6 symmetry axis was also found. The optimized geometries of $(PbS)_n$ nanoparticles (NP) are depicted in Fig. 1.

Total energy calculations were carried out using the VASP 5.4 code [19–21] with the projector-augmented wave method (PAW) [22, 23]. In these calculations, the energy was computed using the generalized gradient approximation (GGA) of DFT as proposed by Perdew, Burke, and Ernzerhof (PBE) [24]. However, standard GGA methods are known to produce too small band gaps due to the incomplete cancelation of the Coulomb self-interaction. For this reason, the screened hybrid functional proposed by Heyd et al. [25] (HSE06 hereafter referred to as HSE), as implemented in the VASP code, that is known to perform extremely well for lead chalcogenides [17] was also used through this work. As the band gaps of bulk lead chalcogenides have been found to be strongly influenced by the magnitude of the spin–orbit coupling of the Pb $6p$ states, their effects on the geometrical and electronic structures of $(PbS)_n$ NPs were also evaluated. In all these calculations, electronic states were expanded using plane wave basis sets with a cutoff of 400 eV. Forces on the ions were calculated through the Hellman–Feynman theorem, including the Harris–Foulkes correction to forces [26]. Iterative relaxation of the atomic positions was stopped when the forces on the atoms were <0.01 eV/Å. Optical spectra were obtained from the frequency-dependent dielectric function, $\varepsilon_2(\omega)$, as proposed by Gajdoš et al. [27]. The $(PbS)_n$ NPs were situated in an orthorhombic cell with a vacuum width of at least 15 Å on each direction. Given the size of these cells, all calculations were performed at the Γ point of the Brillouin zone. The average Pb–S bond energy of all $(PbS)_n$ NP was computed as:

$$E_B = [E_{NP} - nE_{Pb} - nE_S]/n_{bonds}$$

where E_{Pb} and E_S are the corresponding atomic energies, and n_{bonds} is the number of Pb–S bonds on the NP.

3 Results and discussion

Figure 2 shows the average Pb–S distances for the selected $(PbS)_n$ NPs obtained with the different

Fig. 1 Structures of $(PbS)_n$ nanoparticles examined in the present paper and PBE (HSE) relative energies in eV

4a
ΔE=0.00 eV

5a
ΔE = 0.0 eV

6a
ΔE = 0.09 (0.15) eV

6b
ΔE = 0.0 eV

8a
ΔE = 0.49 (0.58) eV

8b
ΔE=0.00 eV

10a
ΔE = 0.27 (0.30) eV

10b
ΔE = 0.50 (0.57) eV

10c
ΔE = 0.27 (0.27) eV

10d
ΔE = 0.74 (0.88) eV

10e
ΔE = 0.91 (1.07) eV

10f
ΔE=0.00 eV

12a
ΔE=0.00 eV

16a
ΔE=0.00 eV

16b
ΔE = 0.61 (0.58) eV

16c
ΔE = 0.19 (0.19) eV

32a
ΔE=0.00 (0.01) eV

32b
ΔE = 0.21 (0.00) eV

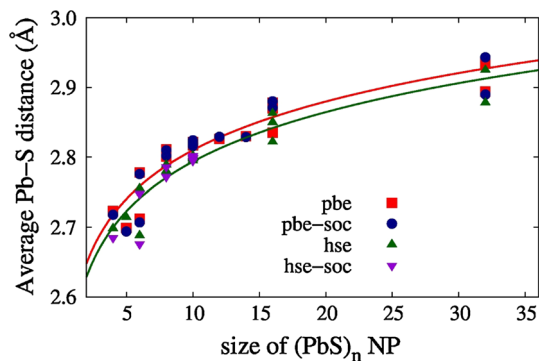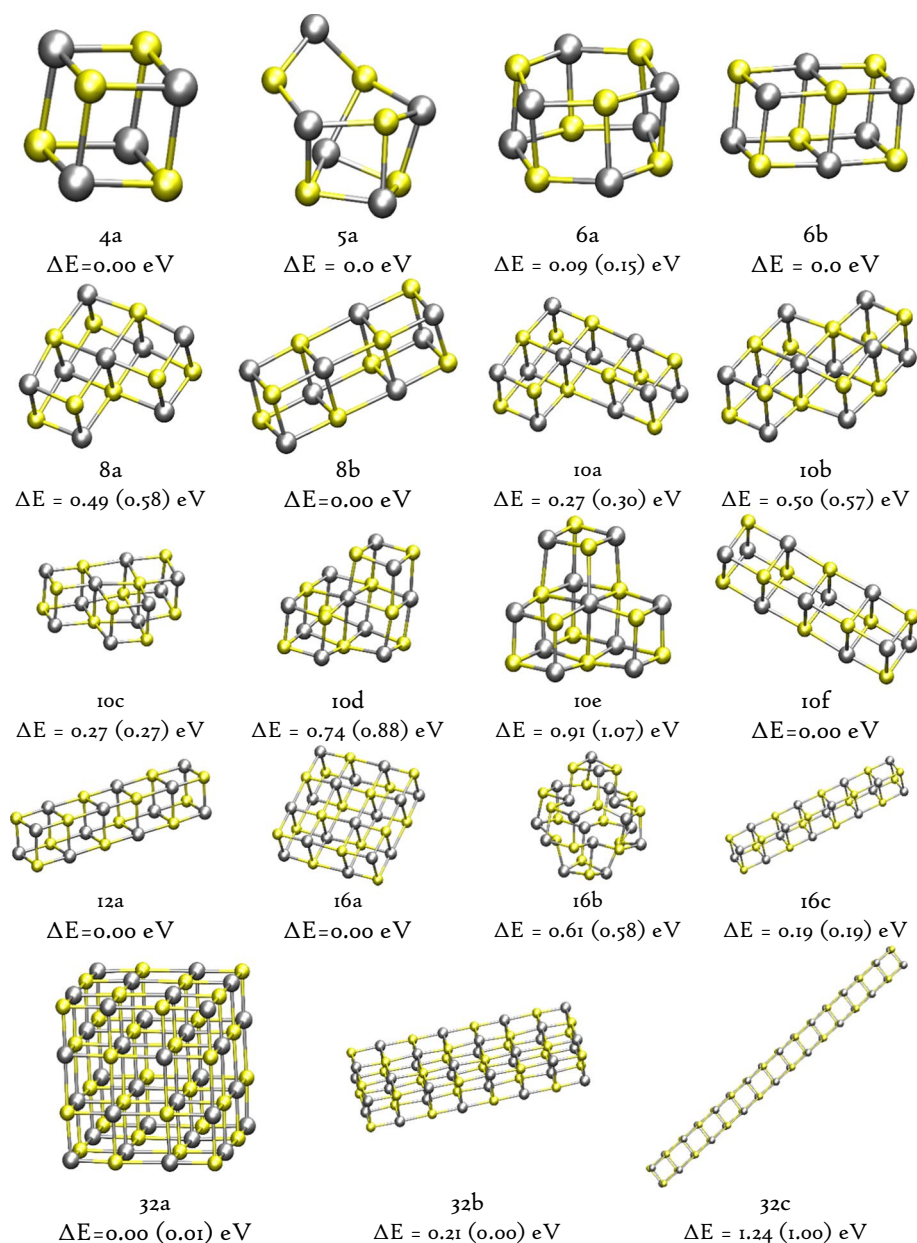32c
ΔE = 1.24 (1.00) eV

Fig. 2 Calculated average Pb–S distances (Å) as a function of increasing NP size

density functionals employed in this study. There is a clear increase in the average Pb–S bond length with increasing NP size from $(PbS)_4$ to $(PbS)_{32}$ in all cases. The inclusion of the computationally expensive spin–orbit coupling terms into the calculations shows to have a negligible effect on the computed Pb–S distances. In no case there is a variation larger than 0.005 Å (PBE) or 0.012 Å (HSE) related to the inclusion of the SOC effects. The trend is the same whether the pure GGA PBE or the hybrid HSE functional is employed to describe the electronic structure of these systems. The only apparent effect is a small shortening of about 0.02 Å in the HSE average Pb–S distances compared with the PBE average distances. This shortening is practically identical to the

effect found in another study of bulk lead chalcogenides that reports Pb–S distances of 3.002 Å (PBE) and 2.9815 Å (HSE03) [17]. As stated previously, the average Pb–S distances increase progressively with increasing NP size; however, a significant variation in individual Pb–S distances within each cluster is found. A closer look at the origin of this behavior shows that it is related to the geometry of the NPs. At corner sites, Pb–S distances (~2.72 Å at PBE) are shorter than at the edges (~2.86 Å), and these are shorter than for hexacoordinated sites (~3.0 Å). Thus, for smaller NPs the average bond distances are shorter, as the proportion of corner and edge sites is higher. As the NP size increases, the proportion hexacoordinated sites increase and, thus, the average Pb–S distance approach that of bulk PbS. However, a detailed examination of the geometries of individual NPs reveals that not all edges or hexacoordinated sites distances are equal. Broadly speaking tricoordinated Pb atoms have two shorter bonds, aprox. 2.68 Å (PBE) and another bond slightly elongated, ~2.79 Å, while in tetracoordinated Pb atoms the shorter bond is ~2.74 Å, there are two longer bonds at ~2.81 Å, and a much longer bond at aprox. 3.2 Å. This behavior has been observed in some lead chalcogenide complexes [28], alkylxanthates, and diethyldithiophosphates [29]. The elongation of the central Pb–S bond in $(PbS)_8$ was already noted in a previous study that used the B3LYP functional [13]. However, there are no references to the observation of the same kind of distortion on higher sizes NP, and there are no details about the remaining Pb–S distances. Similarly, Franceschetti, in its study of PbSe nanoparticles [30], found Pb–Se distances significantly distorted with respect to bulk PbSe, finding a relation to the distance to the nanocrystal surface. However, he used quasi-spherical shape nanoparticles, with significant amounts of low-stability (111) faces present, a factor that may have an important influence in the structural parameters of these NPs.

These distances show that the NPs (except those that show non-cubic geometries) seem to be composed of a collection of $(PbS)_4$ units. That is, the higher size NPs are built in from the addition of a basic unit: the $(PbS)_4$ NP. That must reflect some intrinsic stability of this basic unit. The average Pb–S bond energies plotted in Fig. 3 effectively show a decrease in bond energy with increasing NP size. The bond energy is higher for $(PbS)_4$, 2.77 eV (PBE) or 3.31 eV (HSE) and decreases up to 2.0 eV (PBE) or 2.32 eV (HSE) for the larger NP $(PbS)_{32}$. Previous studies have reported a monotonic increase in binding energies for $n < 5$ and an even–odd oscillation for increasing NP size. This behavior, which seems to be contradictory with our present results, is related to the fact that what these authors present as binding energies are either atomization energies [13] or the average energy needed to decompose the
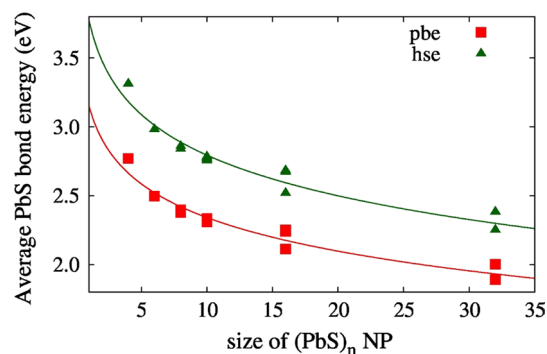

Fig. 3 Computed average bond energy (eV) as a function of increasing NP size

NP into PbS units [14]. The continuous decrease that we observe in the average bond energy can be explained by the higher number of long (thus weaker) Pb–S bonds that appear as the NP size increase. In fact, the $(PbS)_8$ NP can be viewed as the interaction of two $(PbS)_4$ units, and thus, the bond energy of one of those longer bonds can be computed as

$$\Delta E_{bond} = (E_{(PbS)_8} - 2E_{(PbS)_4})/4$$

since there are four of these bonds in the $(PbS)_8$ octamer. From our data, this bond energy can be estimated to be 0.144 eV (0.136 eV) when the PBE (HSE) functional is employed. Similar values are obtained in the larger size NP studied in this work $(PbS)_{32}$, that looks (regarding the Pb–S distances) like a collection of eight of those weakly interacting $(PbS)_4$ units. This means that these longer bonds are intrinsically weak. The reason behind this behavior can be traced to the covalent nature of the PbS bonding in these NP in contraposition to the metallic or extended nature of the bond in bulk PbS. In fact, no distortion in the cubic structure is observed in bulk PbS. Furthermore, the optimization of a lineal infinite $(PbS)_n$ system (with PBC conditions) shows that the geometrical distortion observed in the NP disappears (i.e., all Pb–S distances in the axis direction are identical in this extended system) as the bonding becomes expanded at least in one dimension. This result probably implies that as the NP size increases the inner part of the NP will become more "metallic" while it is logical to assume that the external part will preserve the covalency of the Pb–S bond.

The HOMO–LUMO gaps, presented in Fig. 4, show a general decreasing trend with NP size in agreement with previous studies of other semiconductor NPs. The HSE gaps are higher than those calculated with the PBE functional by 0.7–0.8 eV, but the trend is the same. The inclusion of the SOC effects reduces the gap by 0.5–0.8 eV not only because they split the Pb levels but also because they change the character of the PbS bond. While the
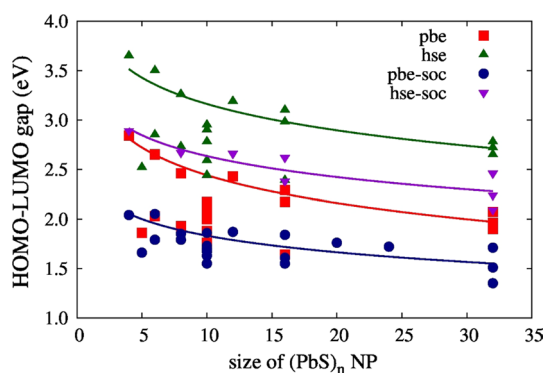
Fig. 4 HOMO–LUMO (eV) gaps as a function of increasing NP size

atoms-projected density of states (DOS) shows that either at the PBE or HSE functionals the occupied levels near the HOMO have similar contributions from both atoms, the inclusion of the SOC effects results in an increased ionicity, with higher energy occupied levels constructed mainly from S levels and lower unoccupied orbitals showing higher Pb contributions.

In both cases (PBE and HSE functionals), there is, for a given NP size, some variations related to the NP geometry. This is quite evident for the $(PbS)_6$ $(PbS)_{10}$, and $(PbS)_{16}$ NPs. This behavior can be related to the NP shape, stability, and number of shorter bonds in the structure. Generally speaking, cubic shape NPs are always more stable than non-cubic ones due to the formation of stronger Pb–S bonds. In consequence structures with weaker and, thus, larger bonds are of lower stability and show a smaller HOMO–LUMO gap. Of the two $(PbS)_6$ NPs, structure 6b is more stable by 0.09 eV when the PBE functional is used (0.15 eV with the HSE functional) and shows a smaller gap of 2.03 eV (2.85 eV) against 2.65 eV (3.50 eV) for structure 6a, which shows hexagonal symmetry. However, in the cubic structure there are only 12 short distances (less than 2.8 Å) while there are 18 short distances in structure 6a, but the longer distance in structure 6a is 2.91 Å while in the cubic structure 6b the longer distance is only 2.70 Å, explaining the lower gap found in this case. The $(PbS)_{10}$ structures are all cubic, e.g., can be constructed by joining together or fusing various $(PbS)_4$ units. The spread of the gap is, now, directly related to the number of shorter bonds. Structures 10d and 10e that present the smaller number of such shorter bonds have the lower gaps, 1.78 eV and 1.88 eV (2.44 eV and 2.59 eV at HSE functional). $(PbS)_{16}$ structures are, again, all derived from $(PbS)_4$ units, and their HOMO–LUMO gaps show a similar behavior than for $(PbS)_{10}$ NPs. The lower energy structure, 16a, is composed of four $(PbS)_4$ units in a plane. Structure 16b is a tridimensional cross-bar structure that results of fusing these four $(PbS)_4$ units in a 3D structure, but the units

are strongly distorted and the structure is the less stable by 0.61 eV (PBE) or 0.58 eV (HSE). Correspondingly, this structure has the higher gap both at the PBE and at the HSE levels. Finally, 16c is a 1D structure formed by the same four $(PbS)_4$ units. This structure is 0.19 eV (both at the PBE and at the HSE levels) higher in energy than the planar structure 16a.

The relative stabilities and gaps of $(PbS)_{32}$ structures deserve a separated comment as Kiran et al. have studied theoretically and by STM and XPS techniques $(PbS)_{32}$ clusters deposited in highly ordered porous graphite (HOPG) [12]. Many of the structures found by these authors in their STM images exhibit square- or rectangular-like shapes. The apparition of those rectangular-shaped images was interpreted as resulting from the addition of two cubic $(PbS)_{32}$ units to form a larger $(PbS)_{64}$ cluster. This interpretation starts from the hypothesis that all $(PbS)_{32}$ units formed and initially deposited on the HOPG surface are cubic-shaped. However, our results allow us to offer a different interpretation as structures 32a (cubic-shaped) and 32b (rectangular) have similar stabilities, while the rod-shaped 32c structure is always higher in energy by about 1 eV. While at the PBE level the cubic structure is more stable by 0.19 eV, at the HSE level both structures are degenerated (32b is more stable by only 0.01 eV). The inclusion of the SOC effects makes the rectangular 2D structure 32b to be more stable by 0.13 eV. Thus, the data of Kiran et al. can be interpreted as resulting from the initial formation and deposition of both 3D and 2D $(PbS)_{32}$ structures on the HOPG surface. Considering the low coverage employed in their experiments the interpretation that we offer here seems to be more plausible than the diffusion of on-surface $(PbS)_{32}$ units that join together to form larger $(PbS)_{64}$ units. The HOMO–LUMO gaps of both structures are quite similar, as expected from their similar relative energies.

The observed dependence of the HOMO–LUMO gaps on the DFT functional employed and on the inclusion of the SOC effects implies that the electronic properties (i.e., the electronic absorption spectrum) will also be strongly dependent on these factors. In particular, Hummer et al. [17] have shown that in bulk lead chalcogenides standard DFT calculations (i.e., using either LDA or GGA approximations to treat the exchange correlation potential) results in negative band gaps and wrong order of band gaps. They also showed that a significant improvement could be obtained by using a hybrid functional and the inclusion of the SOC effects. The comparison of the computed electronic spectra of $(PbS)_{32}$ cubic structure obtained with PBE and HSE functionals and the inclusion of the SOC effects in the latter, presented in Fig. 5, confirm the importance of the use of a hybrid functional. While the onset of absorption starts at ~2 eV when the GGA functional is employed, the electronic absorption spectrum is displaced to higher
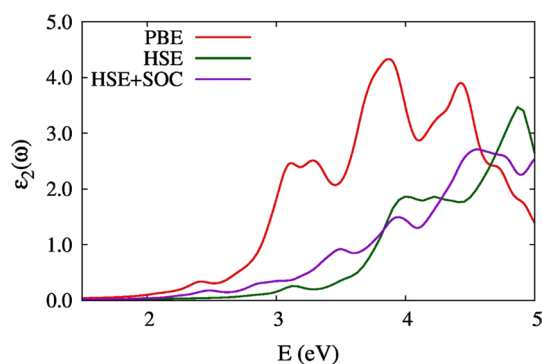
Fig. 5 Computed electronic absorption spectra of $(PbS)_{32}$ cubic structure with different DFT functionals
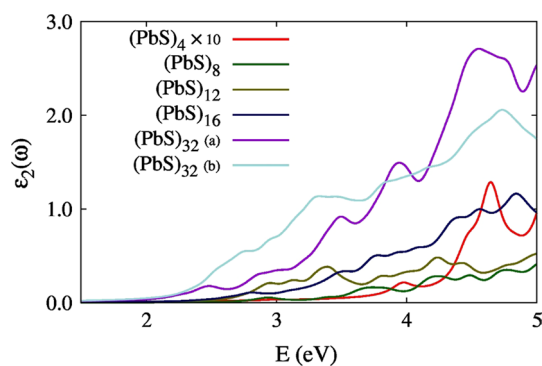

Fig. 6 Computed electronic absorption spectra of different NPs at HSE + SOC level (all spectra normalized to the same cell volume)

energies by about 1 eV when the HSE functional is used. The inclusion of the expensive SOC effects, in turn, displaces the spectrum to lower energies by 0.5 eV but also changes its shape, presenting now a low energy tail that extends to ~2.5 eV the onset of absorption.

The evolution of the electronic absorption spectrum with NP size is presented in Fig. 6. These spectra show the expected evolution toward lower energies with increasing NP size. The most noteworthy feature is the higher energy absorption onset found on $(PbS)_4$ where the first intense maximum is found at ~4.5 eV while for the remaining NPs the comparable onset of absorption starts below 3 eV. In $(PbS)_4$ the DOS shows the LUMO to be found at 2.9 eV, the LUMO + 1 at 3.9 eV and the LUMO + 2 at 4.4 eV. This means that transitions from the HOMO to LUMO or LUMO + 1 are of quite low intensity and that the first clearly allowed transition is the HOMO → LUMO + 2. The spectra presented in Fig. 6 indicate that while $(PbS)_{32}$ NPs present some absorption on the visible region of the spectrum (that extend from 1.65–3.1 eV) larger NP sizes will be required to have intense visible and infrared absorption. We can estimate, from an extrapolation of the logarithmic fitting curve presented in Fig. 4, that to have

a HOMO–LUMO gap, and thus absorption, in the IR/visible limit (1.65 eV) a cubic NP of side length of more than 1.96 nm, ~$(PbS)_{250}$, should be necessary. This result agrees with experimental data that found that PbS NPs of diameter 2.6 nm have a gap of approximately 1.5 eV [31].

4 Conclusions

The structure of $(PbS)_n$ nanoparticles with $n = 4–32$ is found to be quite different from bulk PbS. While in the latter all PbS bonds are equivalent, PbS NPs are found to be made by the successive addition of weakly interacting $(PbS)_4$ units. This results in each hexacoordinated Pb atom having two shorter, two intermediate, and two longer bond, a behavior similar to that observed in molecular complexes with covalent Pb–S bonds.

The distribution of bond distances has its reflection in the electronic structure. While there is a generic trend of HOMO–LUMO gap reduction with increasing NP size, the presence of longer and, thus, weaker bonds on some structures results in particularly low gaps. The choice of the functional used is found to strongly affect the computed electronic structure and, in particular, the inclusion of the SOC effects, while not having a significant effect on the bond distances, reduce the HOMO–LUMO gaps by ~0.5 eV and displace the electronic absorption spectra to lower energies. This confirms the need of accurate DFT calculations based on the HSE functional including the SOC effects to adequately reproduce the electronic structures of these systems. Finally, based on an extrapolation of our hybrid density functional calculations with SOC effects we predict that to have a HOMO–LUMO gap in the IR region of the spectrum (1.65 eV) a cubic NP of at least 1.96 nm side length is required, a result which is in agreement with the experimental observation of band gap of 1.5 eV for PbS QDs of 2.6 nm diameter.

References

1. Carey GH, Abdelhady AL, Ning Z, Thon SM, Bakr OM, Sargent EH (2015) Colloidal quantum dot solar cells. Chem Rev 115:12732–12763
2. Chen G, Seo J, Yang C, Prasad PN (2013) Nanochemistry and nanomaterials for photovoltaics. Chem Soc Rev 42:8304–8338
3. Lee H, Leventis HC, Moon S-J, Chen P, Ito S, Haque SA, Torres T, Nüesch F, Geiger T, Zakeeruddin SM, Grätzel M, Nazeeruddin K (2009) PbS and CdS quantum dot-sensitized solid-state solar cells: old concepts, new results. Adv Funct Mater 19:2735–2742
4. Talapin DV, Lee J-S, Kovalenko MV, Shevchenko EV (2010) Prospects of colloidal nanocrystals for electronic and

optoelectronic nanomaterials for photovoltaics. Chem Rev 110:389–458

5. Zogg H, Maissen C, Masek J, Hoshino T, Blunier S, Tiwari AN (1991) Photovoltaic infrared sensor arrays in monolithic lead chalcogenides on silicon. Semicond Sci Technolog 6:C36–C41

6. Liu S, Tang Z (2010) Nanoparticle assemblies for biological and chemical sensing. J Mater Chem 20:24–35

7. Qiao L-N, Wang HC, Shen Y, Lin Y-H, Nan C-W (2016) Visible-active photocatalytic behaviors observed in nanostructured lead chalcogenides PbX (X = S, Se, Te). AIP Adv 6:015108

8. Hines MA, Scholes GD (2003) Colloidal PbS nanocrystals with size-tunable near-infrared emission: observation of post-synthesis self-narrowing of the particle size distribution. Adv Mater 15:1844–1849

9. Moreels I, Justo Y, Geyter BD, Haustraete K, Martins JC, Hens Z (2011) Size-tunable, bright, and stable pbs quantum dots: a surface chemistry study. ACS Nano 5:2004–2012

10. Sykora M, Koposov AY, McGuire JA, Schultze RK, Tretiak O, Pietryga JM, Klimov VI (2010) Effect of air exposure on surface properties, electronic structure, and carrier relaxation in PbSe nanocrystals. ACS Nano 4:2021–2034

11. Keitel RC, Weidman MC, Tisdale WA (2016) Near-infrared photoluminiscence and thermal stability of PbS nanocrystals at elevated temperatures. J Phys Chem C 120:20341–20349

12. Kiran B, Kandalam AK, Rallabandi R, Koirala P, Li X, Tang X, Wang Y, Fairbrother H, Gantefoer G, Bowen K (2012) $(PbS)_{32}$: a baby crystal. J Chem Phys 136:024317

13. Zeng H, Schelly ZA, Ueno-Noto K, Marynick DS (2005) Density functional study of lead sulfide clusters $(PbS)_n$ ($n = 1$–9). J Phys Chem A 109:1616–1620

14. He J, Liu C, Li F, Sa R, Wu K (2008) Size-dependence of stability and optical properties of lead sulfide clusters. Chem Phys Lett 457:163–168

15. Graciani J, Márquez AM, Plata JJ, Ortega Y, Hernández NC, Meyer A, Zicovich-Wilson CM, Fdez Sanz J (2011) Comparative study of the performance of hybrid DFT functionals in highly correlated oxides: the case of CeO_2 and Ce_2O_3. J Chem Theor Comput 7:56–65

16. Paier J, Marsman M, Hummer K, Kresse G, Gerberm IC, Ángyán JC (2006) Screened hybrid density functionals applied to solids. J Chem Phys 124:154709

17. Hummer K, Grüneis A, Kresse G (2007) Structural and electronic properties of lead chalcogenides from first principles. Phys Rev 75:195211

18. Paier J, Marsman M, Kresse G (2008) Dielectric properties and excitons for extended systems from hybrid functionals. Phys Rev B 78:121201(R)

19. Kresse G, Furthmuller J (1996) Efficient iterative schemes for ab initio total-energy calculations using a plane-wave basis set. Phys Rev B 54:11169–11186

20. Kresse G, Furthmuller J (1996) Efficiency of ab initio total energy calculations for metals and semiconductors using a plane-wave basis set. Comput Mater Sci 6:15–50

21. Kresse G, Hafner J (1993) Ab initio molecular dynamics for liquid metals. Phys Rev B 47:558–561

22. Kresse G, Joubert D (1999) Fast ultrasoft pseudopotentials to the projector augmented-wave method. Phys Rev B 59:1758–1775

23. Blöch PE (1994) Projector augmented-wave method. Phys Rev B 50:17953–17979

24. Perdew JP, Burke K, Ernzerho M (1996) Generalized Gradient Approximation Made Simple. Phys Rev Lett 77:3865–3868

25. Krukau AV, Vydrov OA, Izmaylov AF, Scuseria GE (2006) Influence of the exchange screening parameter on the performance of screened hybrid functionals. J Chem Phys 125:224106

26. Harris J (1985) Simplified method for calculating the energy of weakly interacting fragments. Phys Rev B 31:1770–1779

27. Gajdoš M, Hummer K, Kresse G, Furthmüller J, Bechstedt F (2006) Linear optical properties in the projector-augmented wave methodology. Phys Rev B 73:045112

28. Afzaal M, Ellwood K, Pickett NL, O'Brien P, Raftery J, Waters J (2004) Growth of lead chalcogenide thin films using single-source precursors. J Mater Chem 14:1310–1315

29. Iwasaki H, Hagihara H (1972) The Cristal Structure of Lead (II) Diethyldithiocarbamate. Acta Crystallogr Sect B 28:507–513

30. Franceschetti A (2008) Structural and electronic properties of PbSe nanocrystals from first principles. Phys Rev B 78:075418

31. Choi H, Ko J-H, Kim Y-H, Jeong S (2013) Steric-Hindrace-Driven Shape Transition in PbS Quantum Dots: understanding Size-Dependent Stability. J Am Chem Soc 135:5278–5281